Electronic Supplementary Information

Evaluating the impact of anodic oxidation reactions on water splitting using Prussian blue analog-derived metal-(oxy)hydroxides

Baghendra Singh,[a] Toufik Ansari,[a] Neetu Verma,[a] Yu-Cheng Huang,[b] Pandian Mannu,[b] Chung-Li Dong,[b]* and Arindam Indra[a]*

[a] *Department of Chemistry, Indian Institute of Technology (BHU), Varanasi, UP-221005, India*

E-mail: arindam.chy@iitbhu.ac.in

[b]*Department of Physics, Tamkang University, New Taipei City, Taiwan*

E-mail: cldong@mail.tku.edu.tw

Chemicals

The chemicals were used as received without further purification. $CoCl_2.6H_2O$, NH_2CONH_2, $K_3[Co(CN)_6]$, and methyl alcohol were procured from MERCK Life Sciences Pvt. Ltd., India. NH_4F, and $K_3[Fe(CN)_6]$ were purchased from SRL Pvt. Ltd., India. The benzyl alcohol was procured from Alfa Aesar. Further, *p*-methoxy benzyl alcohol, *p*-methoxy benzyl amine, benzyl amine and ethanol were bought from Avra Synthesis Pvt. Ltd. *p*-methyl benzyl alcohol was purchased from TCI chemicals while hydrazine was bought from Oxford Lab Fine Chemicals. Nickel foam was purchased from Axys Technology, West Bengal, India. Double distilled water was utilized for washing, synthesis and electrochemical measurements.

Instruments

The crystal structure and phases of the synthesized catalysts were evaluated using powder X-ray diffraction pattern (PXRD) conducted on a Rigaku D/MAX RINT-2000 X-Ray diffractometer. The Cu-K_α (λ = 1.5418 Å) radiation was used for the PXRD measurements. The PXRD was recorded in the range of $5° < 2\theta < 80°$.

The IR spectra of the synthesized materials were investigated using Thermo Scientific Nicolet iS5 FTIR spectrometer under attenuated total reflection (ATR) mode.

X-ray photoelectron spectroscopy (XPS) was carried out using VG/VG ESCA LAB 220i X-ray photoelectron spectrometer to evaluate the chemical state, bonding situation, and surface structure of the synthesized catalysts. The XPS data were analyzed using XPS 4.1 software.

The morphology and surface characteristics were investigated by scanning electron microscopy (SEM) using field emission scanning electron microscope EVO-Scanning Electron Microscope MA15/18. Energy dispersive X-ray (EDX) analysis was carried out on Team Pegasus Integrated EDS-EBSD. Transmission electron microscopic (TEM) studies were carried out using Tecnai G2 F30 TWIN transmission electron microscope. A small piece of the catalyst film was sonicated in 2 mL ethanol for 10 min and the well-dispersed particles were drop cast on a Cu grid for the TEM measurements.

The NTEGRA Prima scanning probe microscope was utilized for the atomic force microscopic (AFM) studies.

X-ray absorption spectroscopy

Synchrotron X-ray absorption near-edge structure (XANES) and the Extended X-ray absorption fine structure (EXAFS) were measured at beamline BL17C, which is equipped with a Si(111) double-crystal monochromator at Taiwan Light Source (TLS) of the National Synchrotron Radiation Research Center (NSRRC), Taiwan. The storage ring of TLS operates at 1.5 GeV with a current of about 360 mA. The spectra were collected in transmission mode. Ni foil was used as the reference sample and measured simultaneously downstream so that energy calibration could be performed scan by scan. Raw data were analyzed following standard procedures, including pre-edge and post-edge background subtractions, normalization with respect to the edge jump, and Fourier transformation. The energy resolutions of hard XAS (Co K-edge) and soft XAS (Co L-edge and Fe K-edge) were set to 0.3 and 0.1 eV, respectively.

Experimental

Activation of nickel foam (NF)

1 cm x 2 cm size NF pieces were washed with acetone followed by multiple time washings with double distilled water. The clean NF pieces were sonicated in 1.0 M HCl for 10 min, followed by washings with double distilled water and dried at 50 °C in an air oven for 12 h.

Synthesis of cobalt hydroxide nanoarrays on nickel foam (Co(OH)$_2$@CC)[1]

2 mmol CoCl$_2$.6H$_2$O, 4 mmol NH$_4$F, and 10 mmol NH$_2$CONH$_2$ were dissolved in water (12 mL) to form a mixture. The mixture was transferred into a 40 mL Teflon coated autoclave and pieces of nickel foam were dipped vertically inside the mixture. The autoclave was sealed and heated at 120 °C for 5 h. After normal cooling to room temperature, the freshly prepared films of Co(OH)$_2$@NF were washed with water and ethanol and dried in an air oven at 50 °C for 12 h.

Synthesis of CoFe-PBA@NF

0.4 mmol of K$_3$[Fe(CN)$_6$] was dissolved in 5 mL water in a glass vial to form a clear solution. The pieces of Co(OH)$_2$@NF were immersed vertically inside the solution and kept at room temperature for 1 h. After that, the glass vial was sealed and treated at 60 °C in an air oven for 6 h. As synthesized CoFe-PBA@NF films were washed with water and ethanol several times and dried at 50 °C overnight.

Synthesis of CoCo-PBA@NF

0.4 mmol of K$_3$[Co(CN)$_6$] was dissolved in 5 mL water in a glass vial to form a clear solution. The pieces of Co(OH)$_2$@NF were immersed vertically inside the solution and kept at room temperature for 1 h. The glass vial was sealed and treated at 60 °C in an air oven for 6 h. As synthesized CoCo-PBA@NF films were washed with water and ethanol several times and dried at 50 °C overnight.

Electrochemical transformation of CoFe-PBA@NF and CoCo-PBA@NF

The synthesized precatalyst CoFe-PBA@NF and CoCo-PBA@NF were treated under cyclic voltammetric (CV) conditions using PBAs@NF as working electrode, Hg/HgO as reference electrode, and Pt wire as the counter electrode. The cyclic voltammetry was carried out at the scan rate of 20 mV s^{-1} in the potential range of 1.0-2.0 V vs RHE. After 200 CV cycles, the CoFe-PBA@NF and CoCo-PBA@NF were completely reconstructed into Fe-Co(O)OH@NF and Co(O)OH nanosheets, respectively.

Synthesis of Fe-Co(OH)$_2$-HT@NF[2]

The Fe-Co(OH)$_2$-HT@NF was synthesized by hydrothermal method. A mixture was prepared by dissolving 2 mmol CoCl$_2$.6H$_2$O, 0.4 mmol FeCl$_3$, 4 mmol NH$_4$F and 10 mmol NH$_2$CONH$_2$ in water (12 mL). The mixture was placed into a 40 mL Teflon coated autoclave and pieces of NF were immersed vertically inside the mixture. The autoclave was sealed and heated at 120 °C for 5 h. After normal cooling to room temperature, the synthesized films of Fe-Co(OH)$_2$-HT@NF were washed with water and ethanol and then dried in an air oven at 50 °C for 12 h.

Electrochemical measurements

The electrochemical measurements were performed in a single-compartment three-electrode electrochemical cell in 1.0 M aqueous KOH solution. The catalyst films on carbon cloth were used as the working electrode and Pt wire was used as the counter electrode. Hg/HgO electrode was used as the reference electrode in 1.0 M aqueous KOH solution (pH 13.9). Cyclic voltammetry (CV) and linear sweep voltammetry (LSV) were recorded and represented with 65% iR compensation. All the potentials were represented against reversible hydrogen electrode (RHE) by using the formula:

$$E(RHE) = E(Hg/HgO) + 0.098 + 0.059pH$$

Electrochemical impedance spectroscopic (EIS) measurements were recorded in the frequency range from 0.001 to 100,000 Hz and amplitude of 10 mV. The charge transfer resistance (R_{ct}) was calculated from the diameter of the semicircle in the Nyquist plots

The chronoamperometric measurements (CA) were carried out in 1.0 M aqueous KOH at selected constant potentials and represented without iR compensation. Tafel plots were determined by potentiostatic measurements at the potentials where current density was reached up to 10 mA cm^{-2}. The Tafel slope was calculated using the Tafel equation:

$$\eta = b \log j + a$$

where η denotes the overpotential (V), j is the current density (mA cm^{-2}), and b is the Tafel slope (mV dec^{-1}). The electrochemically active surface areas (ECSAs) were evaluated by determining the double-layer capacitance (C_{dl}). For C_{dl} measurements, CV was carried out at a potential range, where no apparent faradaic process occurred. The ECSA of the catalysts was determined by the equation ECSA = C_{dl} / C_s where C_s represents the specific capacitance of the material for a standard with 1 cm^2 of the real surface area under identical electrolyte conditions.

Conditions for Benzyl alcohol oxidation

It should be mentioned here that the BA oxidation should be operated at the potential lower than the onset of OER to avoid the interference from OER. As the Fe-Co(O)OH showed onset potential of 1.53 V vs RHE for OER, the electrochemical oxidation of benzyl alcohol was performed in a three electrode system (Fe-Co(O)OH as working electrode, Pt wire as counter electrode and Hg/HgO as reference electrode) at a constant potential of 1.50 V vs RHE for 3 h under chronoamperometric conditions. The BA oxidation was performed in a 10 mL customized electrochemical cell.

As the high conversion and faradaic efficiency was observed at 1.50 V vs RHE, the BA oxidation was carried out using Co(O)OH and hydrothermally prepared Fe-Co(O)OH-HT under the similar reaction conditions and the superiority of PBA-derived Fe-Co(O)OH was established. After the complete reaction, the product was extracted by toluene and further analyzed by the ^{1}H NMR spectroscopy.

Separation of benzoic acid

The benzoic acid formed after BA oxidation is converted into potassium benzoate (Ph-COOK) in KOH solution. Therefore, the electrolyte solution was neutralized by the addition of 3.0 M HCl after the

completion of the reaction while Ph-COOK was converted into Ph-COOH. The Ph-COOH crystals having KCl were filtered and recrystallization in hot water was repeated to remove KCl from Ph-COOH. For recrystallization, the obtained crystals were dissolved in hot double distilled water (80 °C) and cooled down naturally. After cooling, high-purity Ph-COOH was recrystallized and collected by the filtration.

Determination of Faradaic efficiency for BA oxidation

The Faradaic efficiency was determined on the basis of the weight of the BA and the charge passed through during the electrocatalytic reaction. As the full conversion of BA into benzoic acid was confirmed by ^{1}H NMR spectra, the required charge for full conversion ($Q_{100\% FE}$) was calculated by:

$$Q_{100\% FE} = \frac{m_{BA} \times F \times n_e}{M_{BA}}$$

where F is the Faraday constant (96485 C mol^{-1}), n_e denotes the number of electrons required for the oxidation process (4), m_{BA} is the weight of BA used for the reaction (112.32 mg) and M_{BA} is the molecular weight of BA (108.14 g mol^{-1}). The calculation results $Q_{100 \% FE}$ = **400.85 C**. When the purity of the BA (99% Alfa Aesar) is considered, the $Q_{100 \% FE}$ is reduced to **396.84 C**. After 3 h, the charge passed through the potentiostat for the full conversion of BA is calculated to be **392.50 C**. The quotient of these charges results in the Faradaic efficiency of 98.9% after 3 h.

It should be mentioned here that we have provided the conversion and selectivity as well as NMR data of isolated products. The previous studies have established that the researchers have given the preference to isolated yield in contrast to the NMR yield.[3-5] It has been established that after the completion of reaction, if we got enough amount of product (above 10 mg) it is better to calculate the isolated yield with percentage of conversion. As we have obtained more than 10 mg of product, we have calculated the isolated yield and further selectivity was determined. Further, we have provided the NMR data of the isolated product. The isolated yield can be calculated by the following formula:

Yield (%) = (actual number of moles/theoretical number of moles) x 100

The selectivity was determined by the formula:

$$Selectivity\ (\%) = \frac{moles\ of\ desired\ oxidized\ product}{(moles\ of\ substrate\ used) - (moles\ of\ substrate\ left\ after\ reaction)} \times 100$$

Measurement of produced hydrogen

The generated hydrogen during OER and AORs was measured using a H-type cell by water-displacement method in a two electrode system. The chronoamperometry was carried out at the potential of 1.50 V for 30 min. The generated hydrogen gas in mL was converted into mmol.
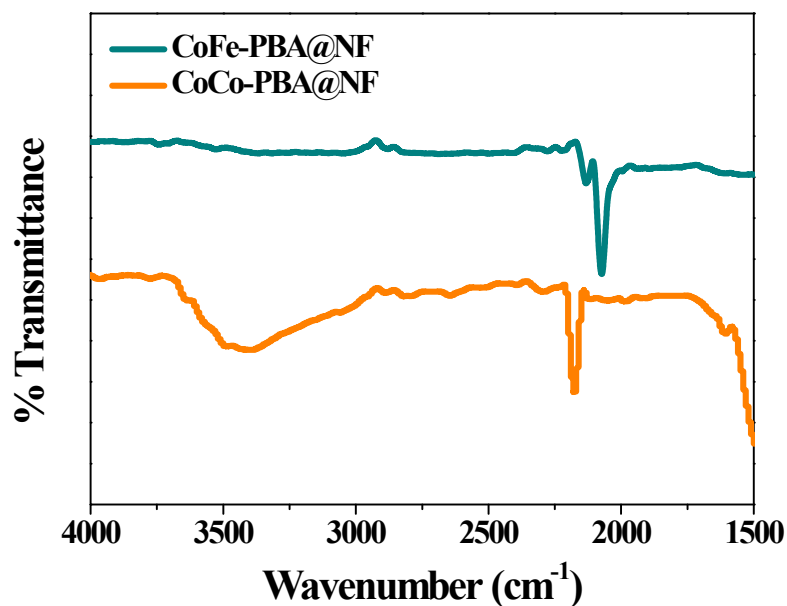
Figures

Figure S1. IR spectra of CoFe-PBA@NF and CoCo-PBA@NF. The peaks at 2170 cm^{-1} in CoCo-PBA@NF and 2130 cm^{-1} in CoFe-PBA@NF were assigned for the asymmetric stretching vibrations of bridging –CN groups.[1,6]
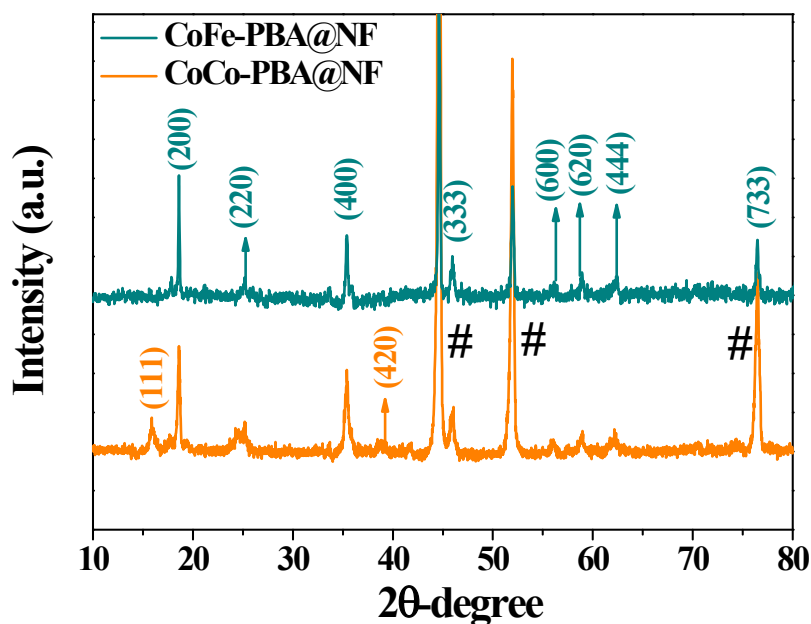

Figure S2. The PXRD pattern of CoFe-PBA@NF and CoCo-PBA@NF. The peaks were well indexed and assigned for the cubic crystal system [space group Fm3m (225)] matched with the JCPDF No.-01-077-1161. The # marked peaks are the characteristic peaks of *fcc* Ni (nickel foam).
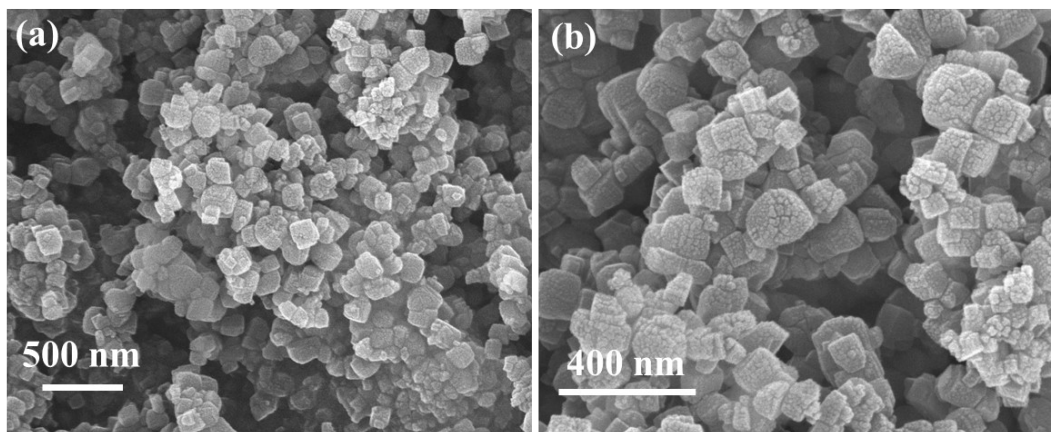
Figure S3. (a-b) SEM images of CoFe-PBA@NF at different resolutions showing the cubic morphology.
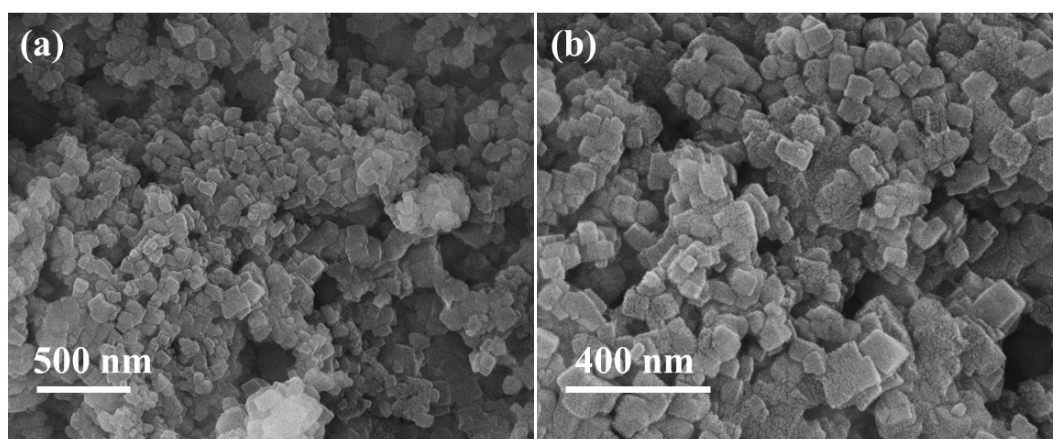
Figure S4. (a-b) SEM images of CoCo-PBA@NF at different resolutions showing the cubic morphology.
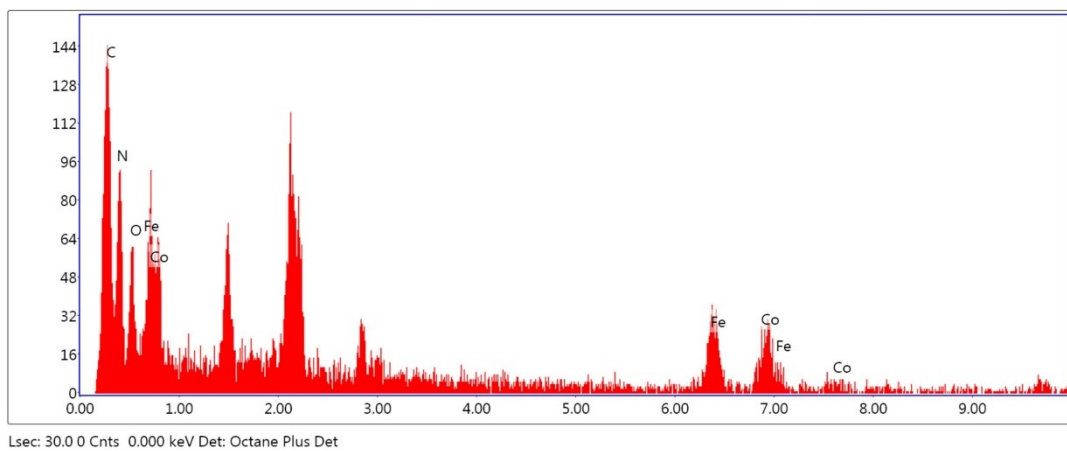
Figure S5. EDX spectrum of CoFe-PBA@NF showing the presence of Co, Fe, C, N and O.
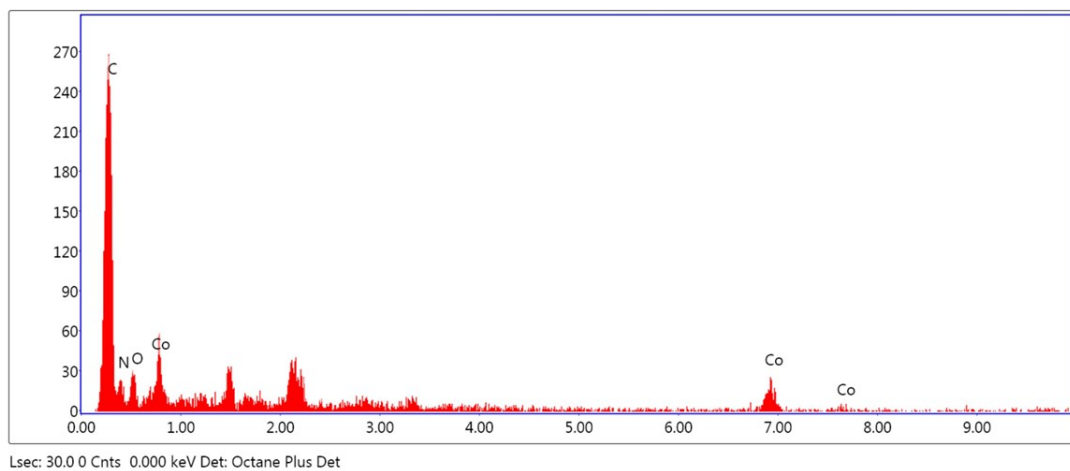
Figure S6. EDX spectrum of CoCo-PBA@NF showing the presence of Co, C, N and O.
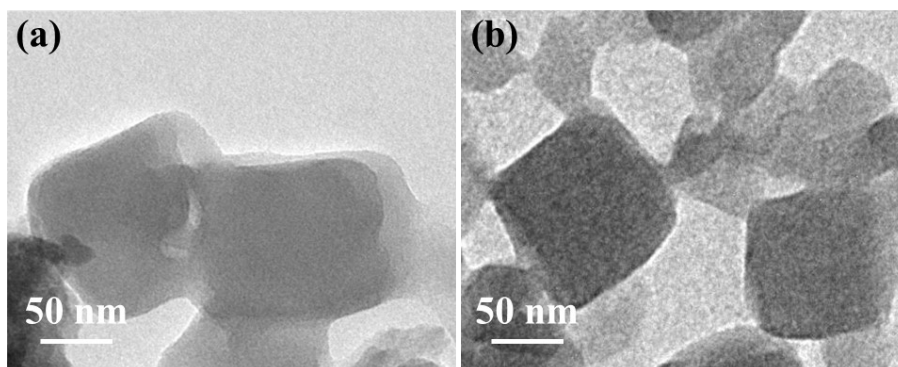
Figure S7. TEM images of (a) CoFe-PBA and (b) CoCo-PBA indicating the cubic morphology.
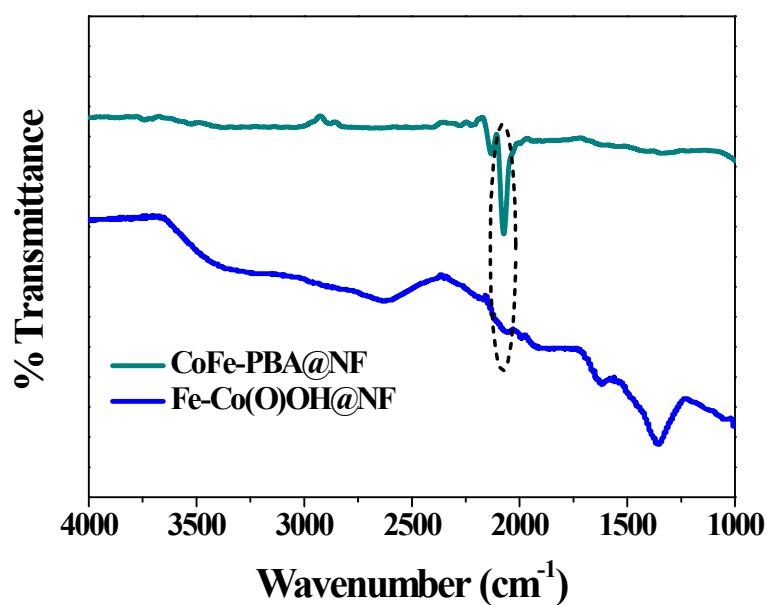
Figure S8. IR spectra of CoFe-PBA@NF and electrochemically reconstructed Fe-Co(O)OH@NF. The peaks corresponding to the asymmetric stretching vibrations of bridging –CN group completely disappeared after electrochemical reconstruction.[1,6]
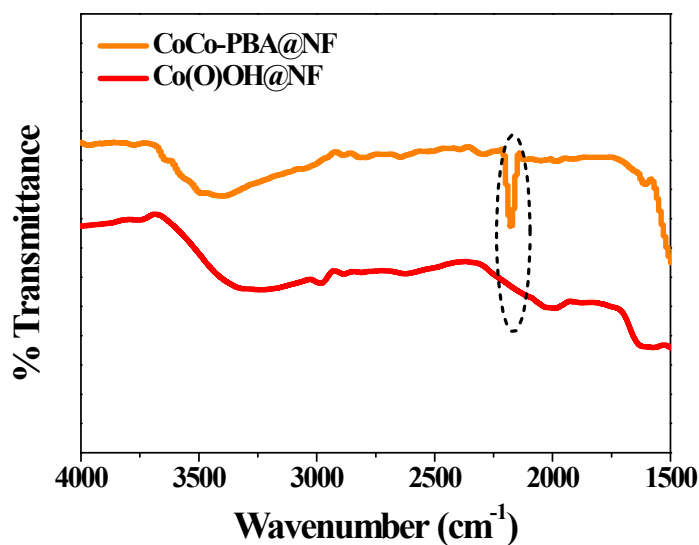
Figure S9. IR spectra of CoCo-PBA@NF and electrochemically reconstructed Co(O)OH@NF. The peaks corresponding to the asymmetric stretching vibrations of bridging –CN group completely disappeared after electrochemical reconstruction.[1,6]
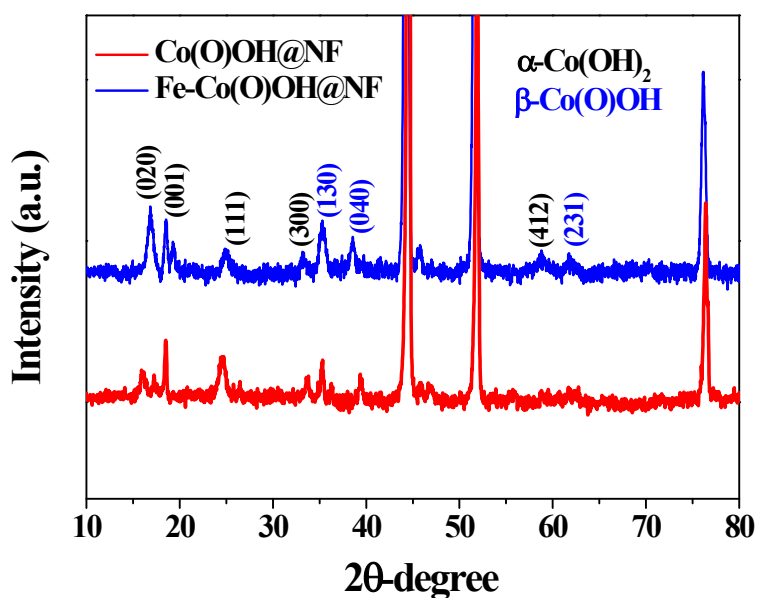
Figure S10. PXRD pattern of electrochemically reconstructed Fe-Co(O)OH@NF and Co(O)OH@NF catalysts. The peaks were well indexed and assigned for the mixed phase of α-Co(OH)$_2$ (JCPDF No.-48-0083) and β-Co(O)OH (JCPDF No.-26-0480).
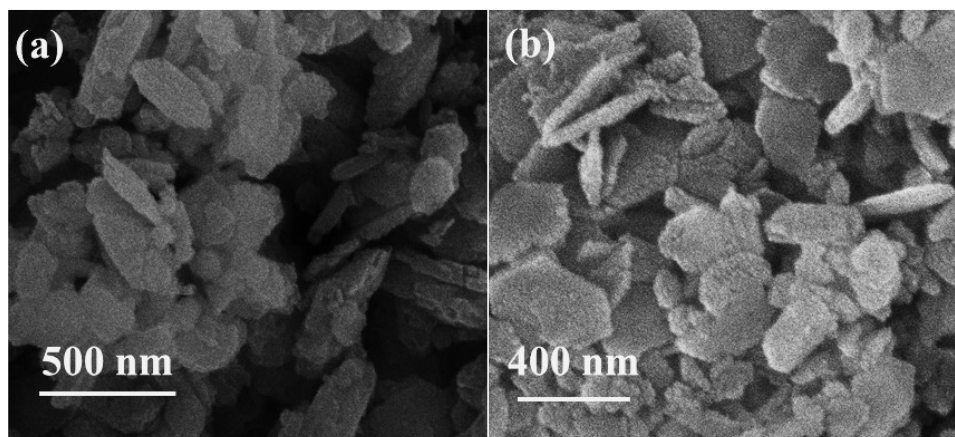
Figure S11. (a-b) SEM images of electrochemically reconstructed Co(O)OH@NF catalyst at different resolutions showing the nanoplate like morphology.
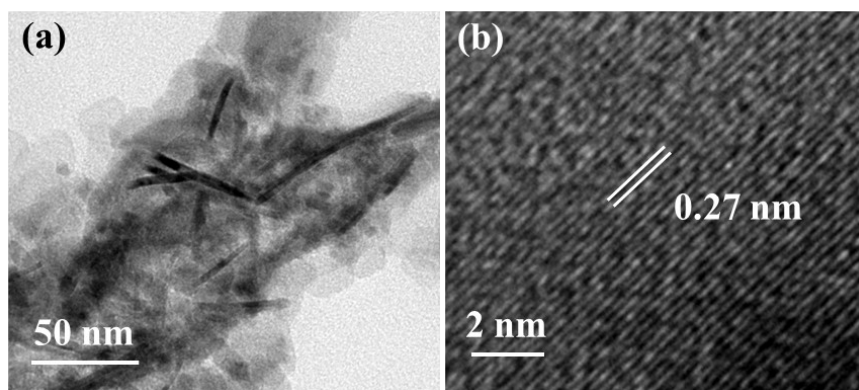
Figure S12. (a) TEM image of electrochemically reconstructed Co(O)OH catalyst showing the nanosheet morphology and (b) corresponding HRTEM image detecting the d-spacing of 0.27 nm corresponded to the (001) plane of β-Co(O)OH (JCPDF No.-26-0480).
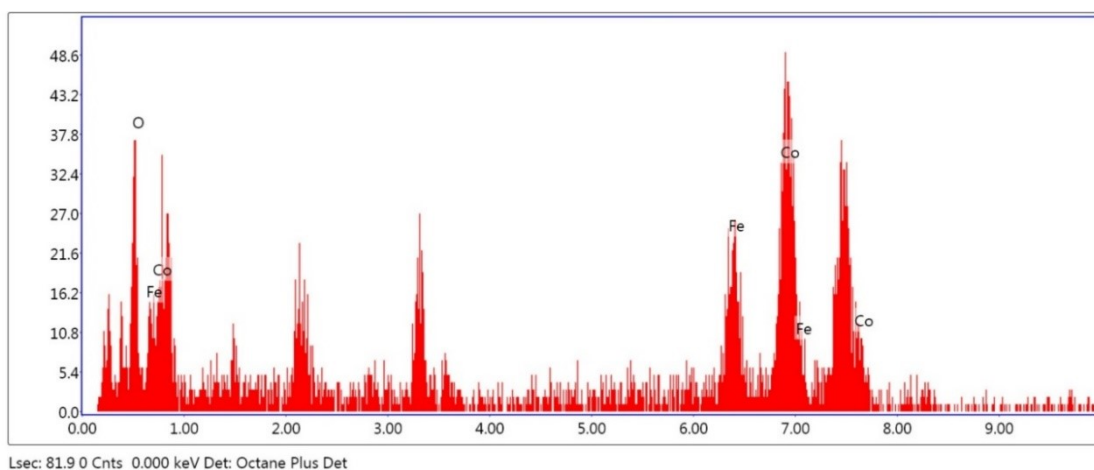
Figure S13. EDX spectrum of electrochemically reconstructed Fe-Co(O)OH catalyst indicating the existence of Co, Fe and O elements.
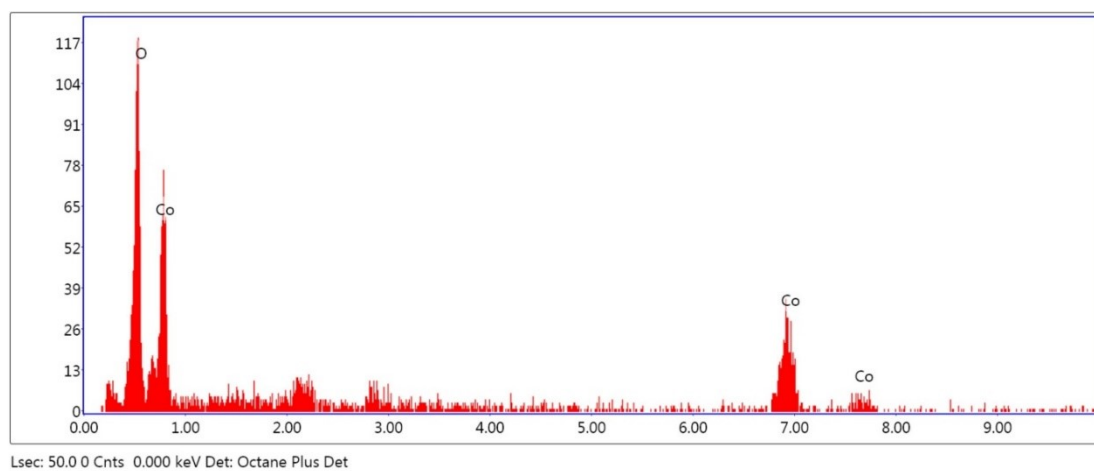
Figure S14. EDX spectrum of electrochemically reconstructed Co(O)OH catalyst showing the presence of Co and O.
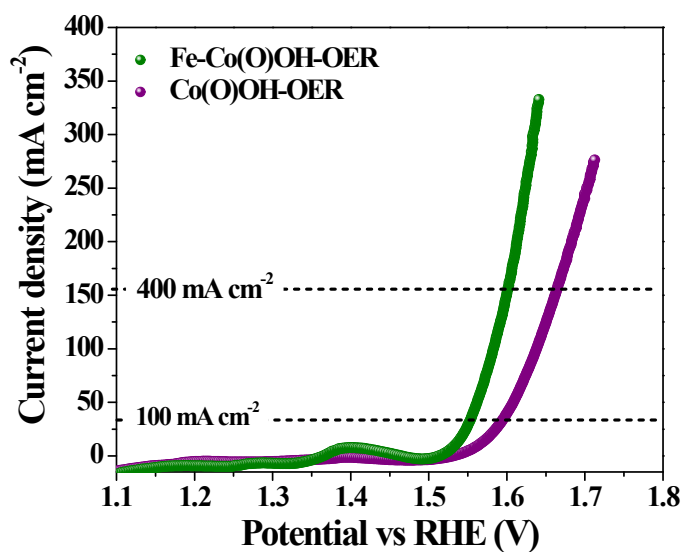
Figure S15. LSV profiles for the OER of electrochemically reconstructed Fe-Co(O)OH compared with Co(O)OH showing the superior OER activity of Fe-Co(O)OH.
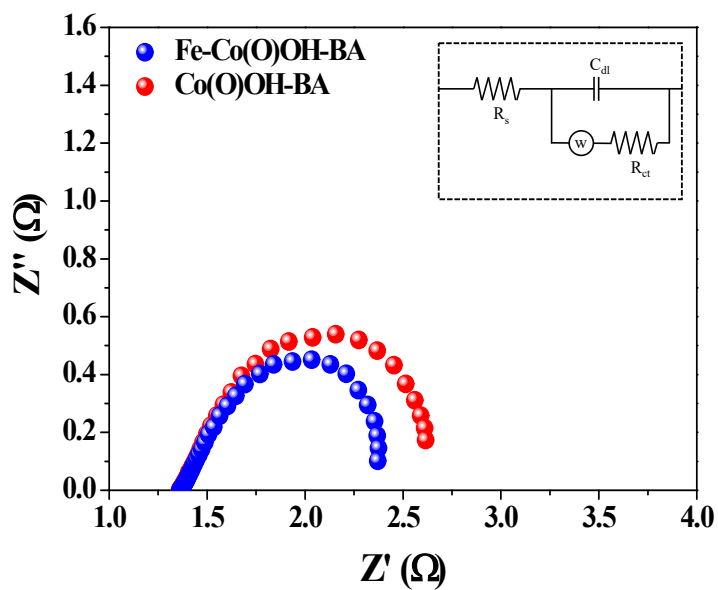

Figure S16. EIS spectra of Fe-Co(O)OH compared with Co(O)OH showing the lower charge transfer resistance.

The formation of semicircles in EIS depends on the nature of circuit used to record the impedance data. To determine the best equivalent circuit of an electrochemical system, the impedance over a range of frequencies needs to be measured. The previous studies have shown that most of the electrochemical systems can be explained quite well by recording impedance data in the frequency range of 0.001 Hz to 1×10^4 Hz. Electrochemical impedance plots may have several semicircles or a single semicircle. The formation of single semicircle indicates that only one rate determining step is involved in the electrochemical process with a single time constant. For some electrochemical processes, more than one rate-determining step may contribute to the to the overall reaction rate constant and hence impedance component to get multiple time-constant Nyquist plot.

We have performed the impedance in the frequency range of 0.001 Hz to 1×10^4 Hz and only single semicircle is visible. Accordingly, we have fitted the circuit. As the formation of semicircle is directly related to the number of rate-detemining step (time constant) in a particular electrochemical process, the formation of single semicircle described the one rate-determining step in the electrochemical process.
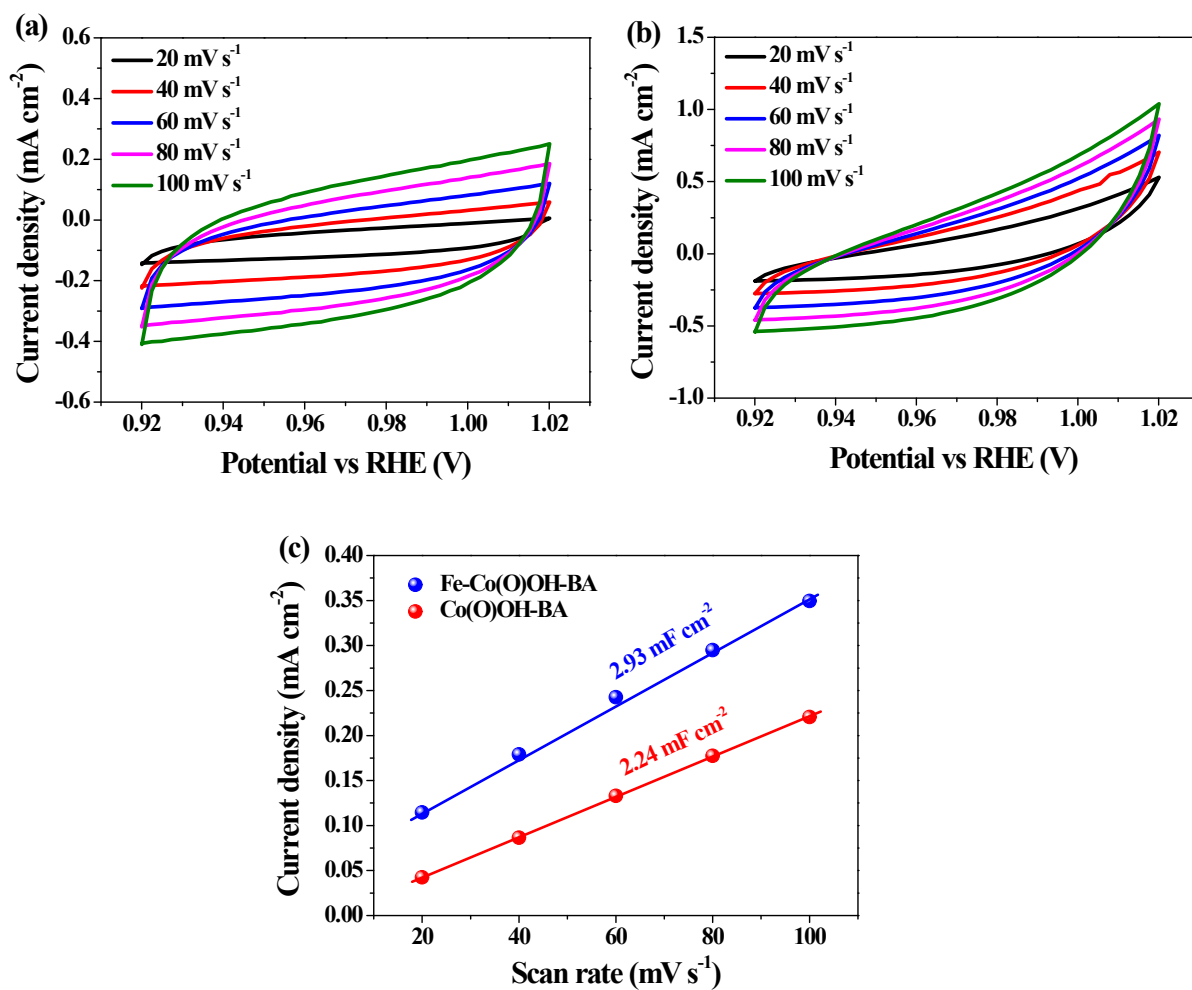
Figure S17. Cyclic voltammetry in the non-faradaic region for the determination of double layer capacitance (C_{dl}) of electrochemically reconstructed (a) Co(O)OH nanosheets and (b) Fe-Co(O)OH nanosheets and (c) C_{dl} plot showing the largest C_{dl} of Fe-Co(O)OH-BA.[7,8]

Table S1. Comparison of BA oxidation activity of Fe-Co(O)OH with literature reported catalysts.

| Sr. No.	Catalyst	Potential	Current density	Faradaic efficiency	Reference
1.	Fe-Co(O)OH	1.47 V vs RHE	400 mA cm^{-2}	98.3%	*This work*
2.	$CoFeO_x$	1.42 V vs RHE	50 mA cm^{-2}	95%	*ACS Energy Lett.* **2018**, *3*, 1854-1860.
3.	$Co_{0.83}Ni_{0.17}$/AC	1.425 V vs RHE	10 mA cm^{-2}	96%	*New J. Chem.* **2018**, *42*, 6381-6388.
4.	Co_3O_4	1.50 V vs RHE	86 mA cm^{-2}	91.4%	*J. Mater. Sci.* **2021**, *56*, 6689-6703.
5.	NiCo-21-MOF	1.52 V vs RHE	338.16 mA cm^{-2}	-	*Inorg. Chem.* **2022**, *61*, 7308-7317.
6.	ZIF-9@GO	1.60 V vs RHE	204 mA cm^{-2}	88%	*J. Mater. Chem. A* **2024**, *12*, 233-246.
7.	NiO/Ni_3S_2	1.609 V vs RHE	50 mA cm^{-2}	94%	*Chem. Eng. J.* **2022**, *431*, 134137.
8.	$NC@CuCo_2N_x$	1.25 V vs RHE	10 mA cm^{-2}	81.3%	*Adv. Funct. Mater.* **2017**, 1704169
9.	Ni_2P	1.30 V vs RHE	10 mA cm^{-2}	95.3%	*J. Colloid Interface Sci.* **2023**, *640*, 329-337.
10.	$NiCo_2O_4$	1.46 V vs RHE	100 mA cm^{-2}	99%	*Inorg. Chem. Front.* **2023**, *10*, 2053-2059.
11.	$Ni@Ni/NiO_x$	1.309 V vs RHE	10 mA cm^{-2}	96%	*Chem. Eng. J.* **2023**, *453*, 139797.
12.	NiCo-hydroxide	1.35 V vs RHE	100 mA cm^{-2}	95%	*Energy Environ. Sci.* **2020**, *13*, 4990-4999.
13.	$ZnCo_2O_4$ $@Ni(OH)_2$	1.48V vs RHE	100 mA cm^{-2}	96%	*Int. J. Hydro. Energy* **2024**, *49*, 228-237.
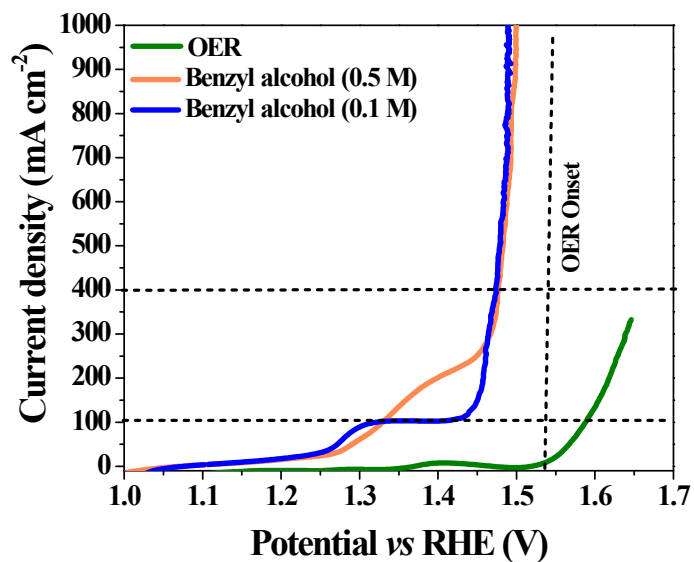
Figure S18. Comparison of LSV profiles for 0.1 M BA oxidation and 0.5 M BA oxidation using Fe-Co(O)OH catalyst.
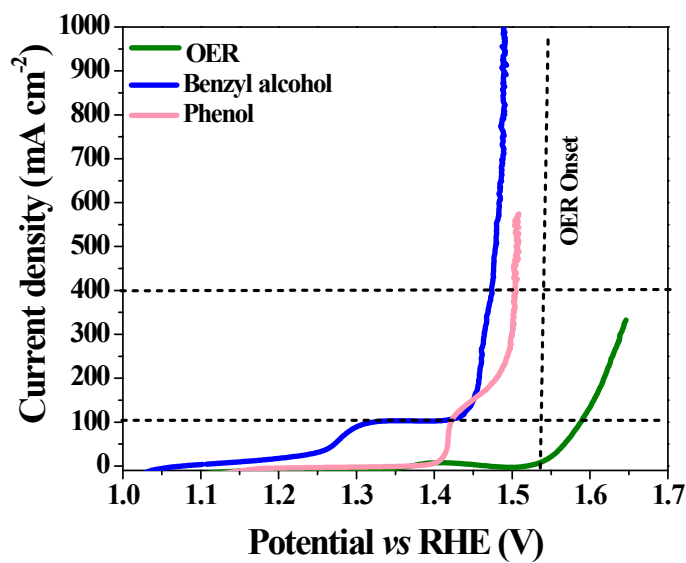

Figure S19. Comparison of LSV profiles for BA oxidation, phenol oxidation as well as for OER using Fe-Co(O)OH catalyst.
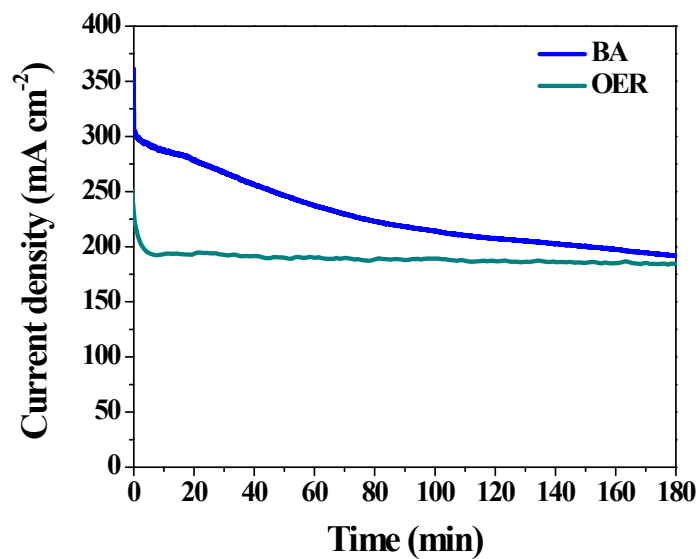
Figure S20. Chronoamperometric measurements carried out at 1.50 V vs RHE potential for BA oxidation as well as for OER using Fe-Co(O)OH catalyst.
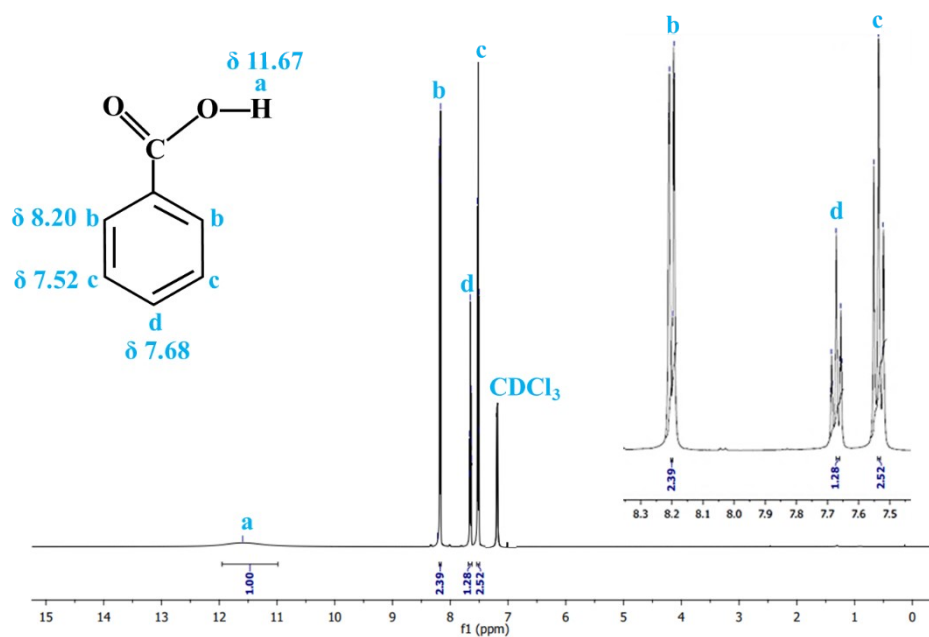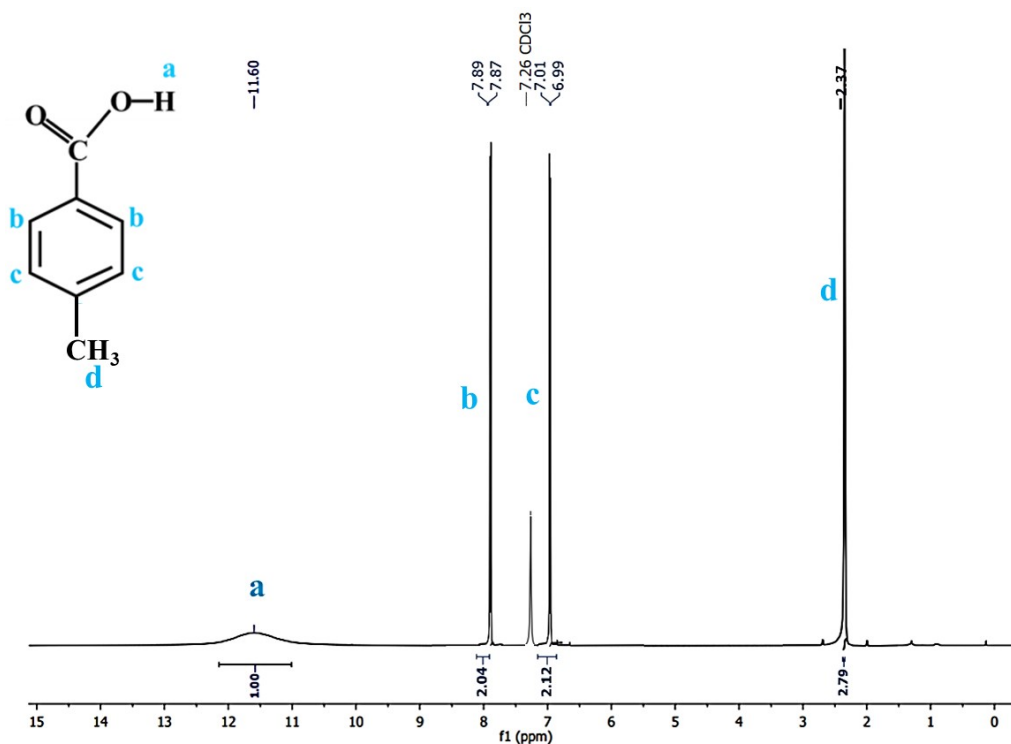

Figure S21. ^{1}H NMR spectra of benzoic acid obtained after 3 h of anodic oxidation of benzyl alcohol at 1.50 V vs RHE potential using Fe-Co(O)OH.
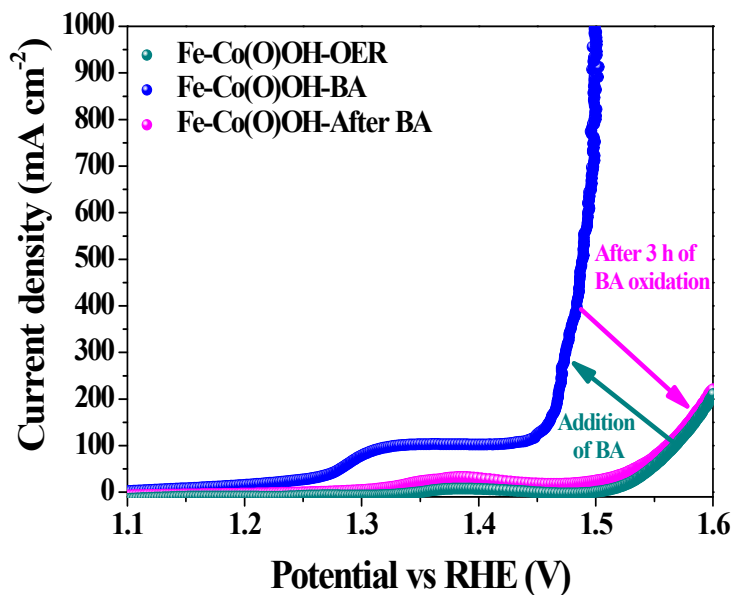
**Figure S22.** LSV profiles for the OER, BA oxidation, and after 3 h of the BA oxidation using electrochemically reconstructed Fe-Co(O)OH. The LSV profile indicated a similar LSV curve for OER and after 3 h of BA oxidation showing that the OER was started after the complete oxidation of BA at 3 h.

Figure S23. ^{1}H NMR spectra of *p*-methyl benzoic acid obtained after 3 h of anodic oxidation of *p*-methyl benzyl alcohol at 1.50 V vs RHE using Fe-Co(O)OH.
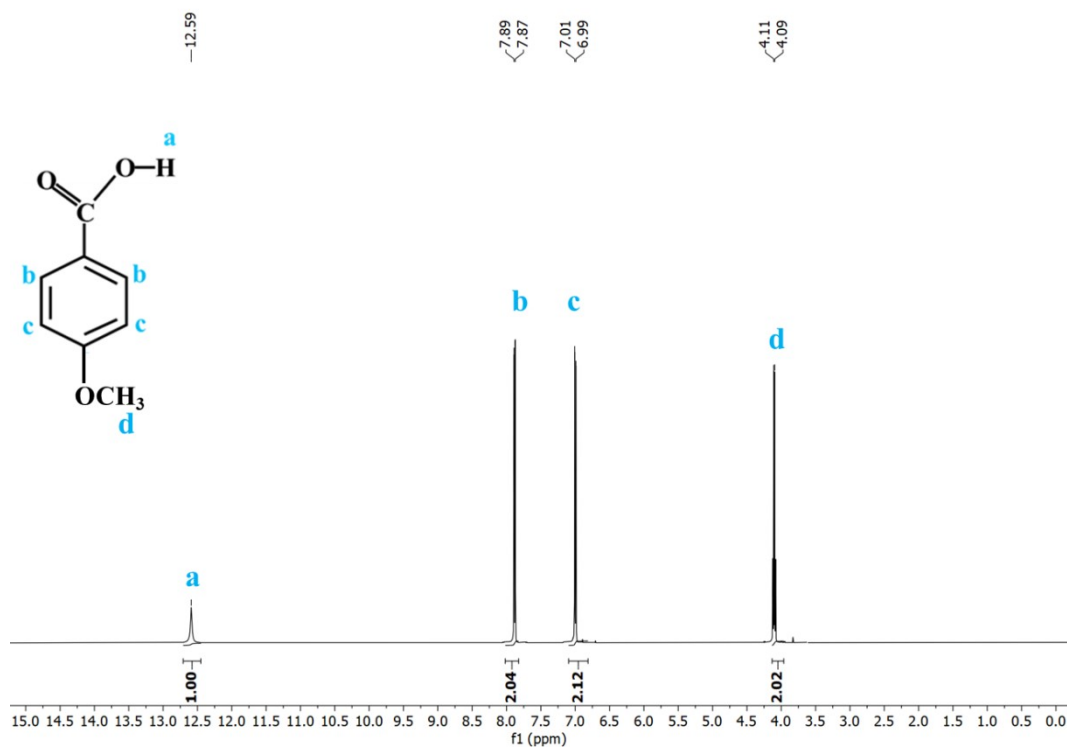
Figure S24. ^{1}H NMR spectra of *p*-methoxy benzoic acid obtained after 3 h of anodic oxidation of *p*-methoxy benzyl alcohol at 1.50 V vs RHE using Fe-Co(O)OH.
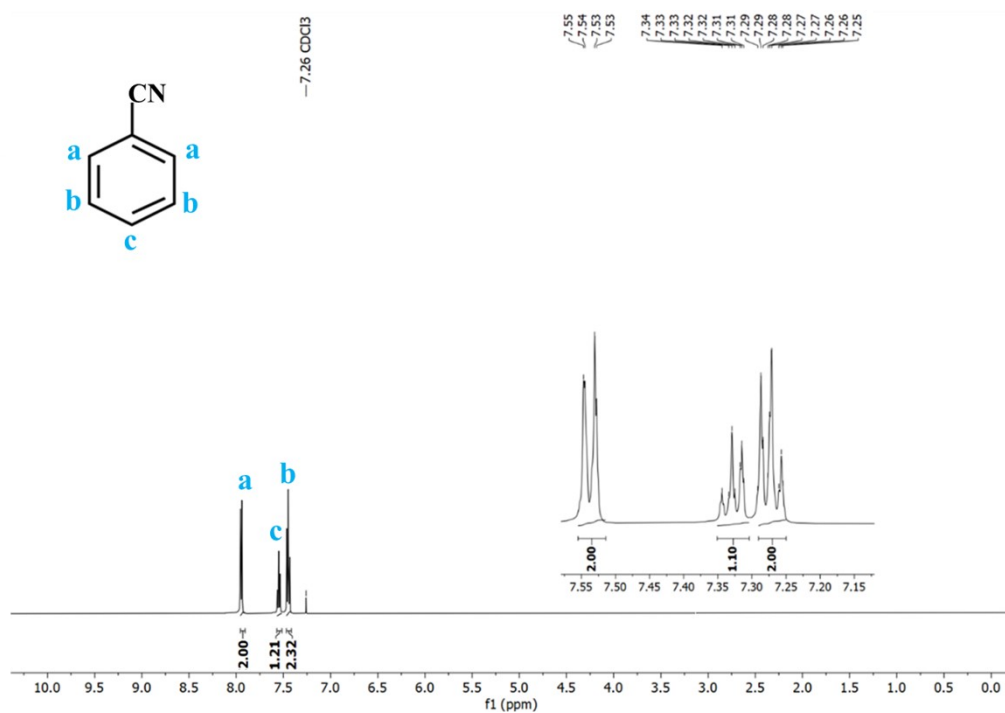

Figure S25. ^{1}H NMR spectra of benzonitrile obtained after 3 h of anodic oxidation of benzylamine at 1.50 V vs RHE using Fe-Co(O)OH.
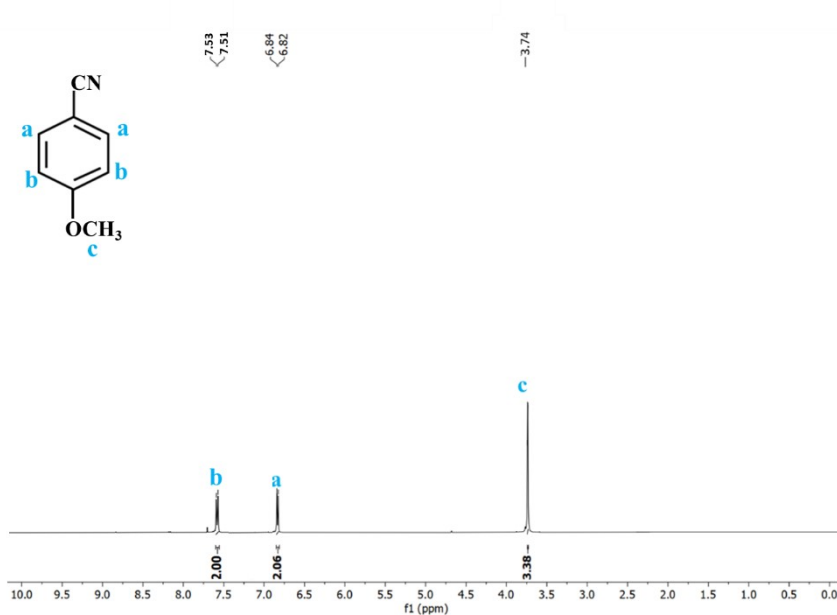
20

Figure S26. ^{1}H NMR spectra of *p*-methoxy benzonitrile obtained after 3 h of anodic oxidation of *p*-methoxy benzylamine at 1.50 V vs RHE using Fe-Co(O)OH.
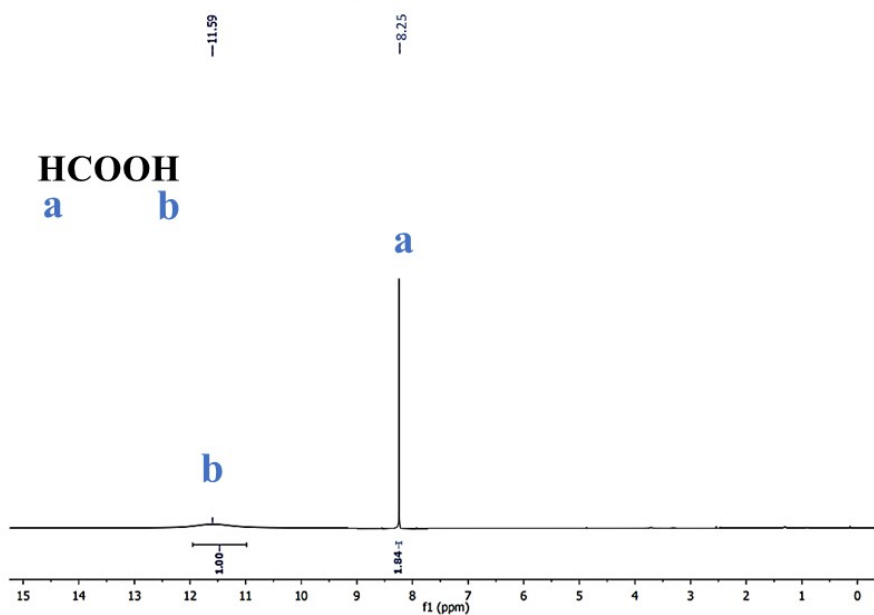

Figure S27. ^{1}H NMR spectra of formic acid obtained after 3 h of anodic oxidation of methyl alcohol at 1.50 V vs RHE using Fe-Co(O)OH.
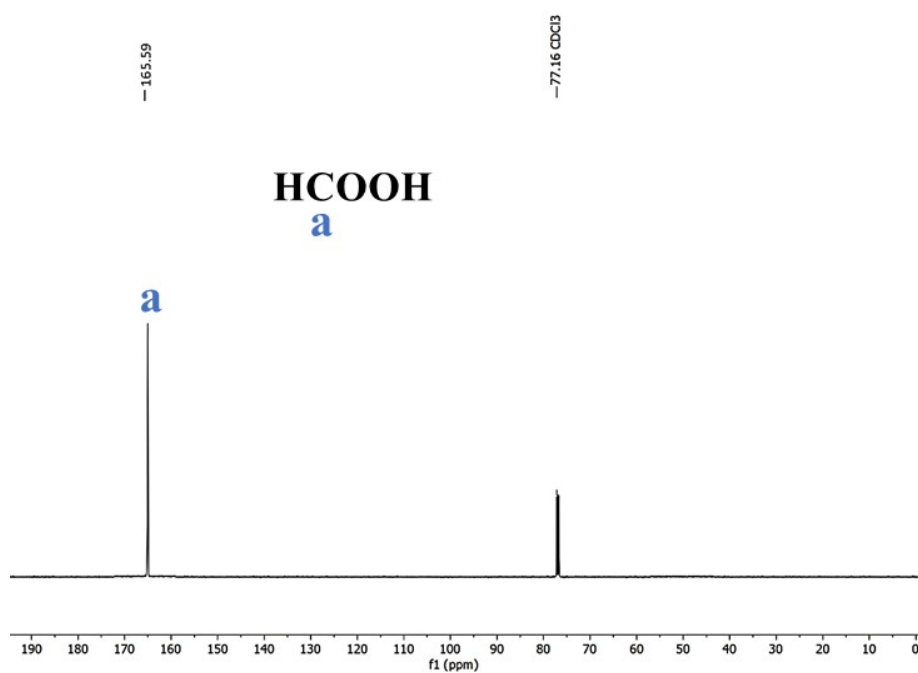
Figure S28. ^{13}C NMR spectra of formic acid obtained after 3 h of anodic oxidation of methyl alcohol at 1.50 V vs RHE using Fe-Co(O)OH.
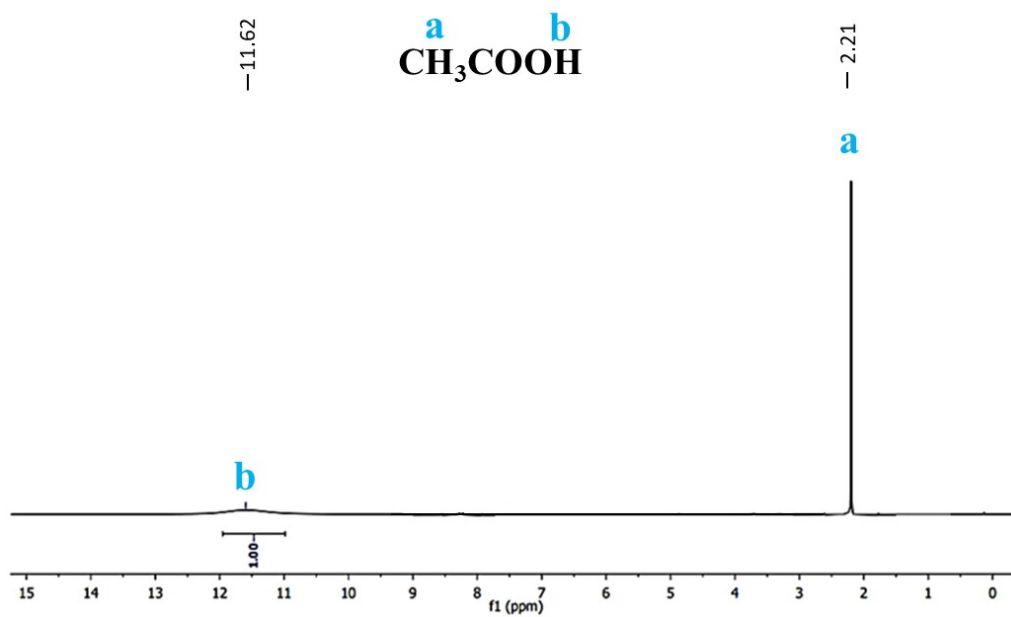

Figure S29. ^{1}H NMR spectra of ethanoic acid obtained after 3 h of anodic oxidation of ethyl alcohol at 1.50 V vs RHE using Fe-Co(O)OH.
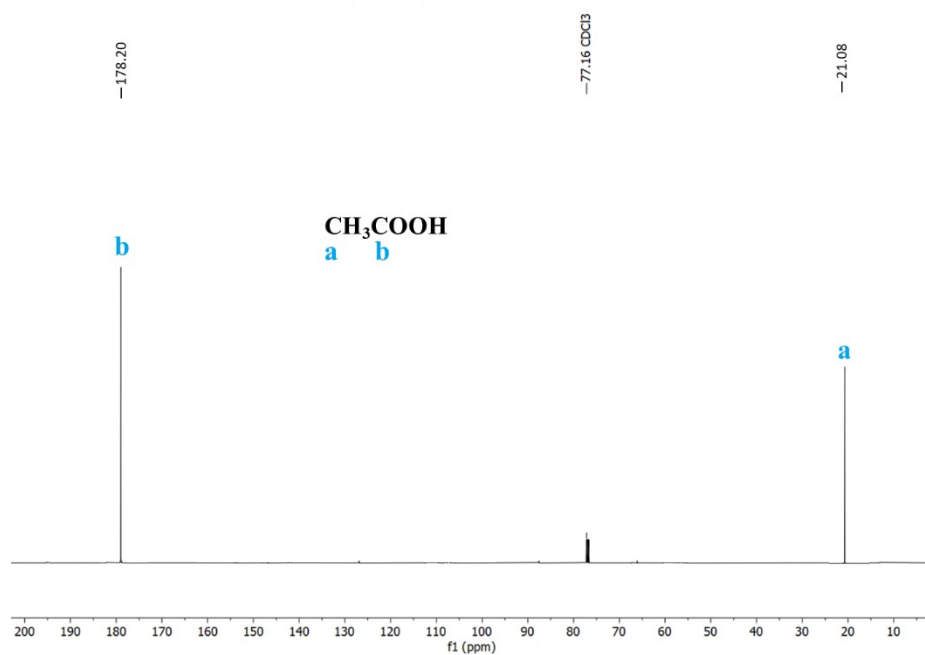
Figure S30. ^{13}C NMR spectra of ethanoic acid obtained after 3 h of anodic oxidation of ethyl alcohol at 1.50 V vs RHE using Fe-Co(O)OH.
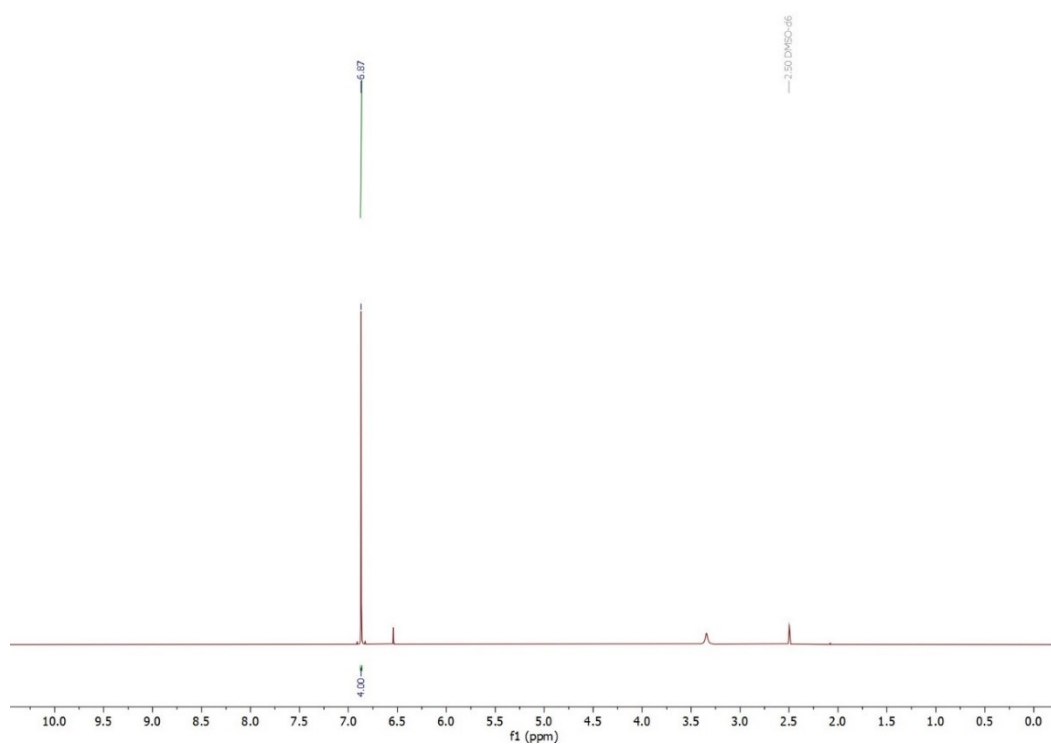

Figure S31. ^{1}H NMR spectra of benzoquinone obtained after 3 h of anodic oxidation of phenol at 1.50 V vs RHE potential using Fe-Co(O)OH.
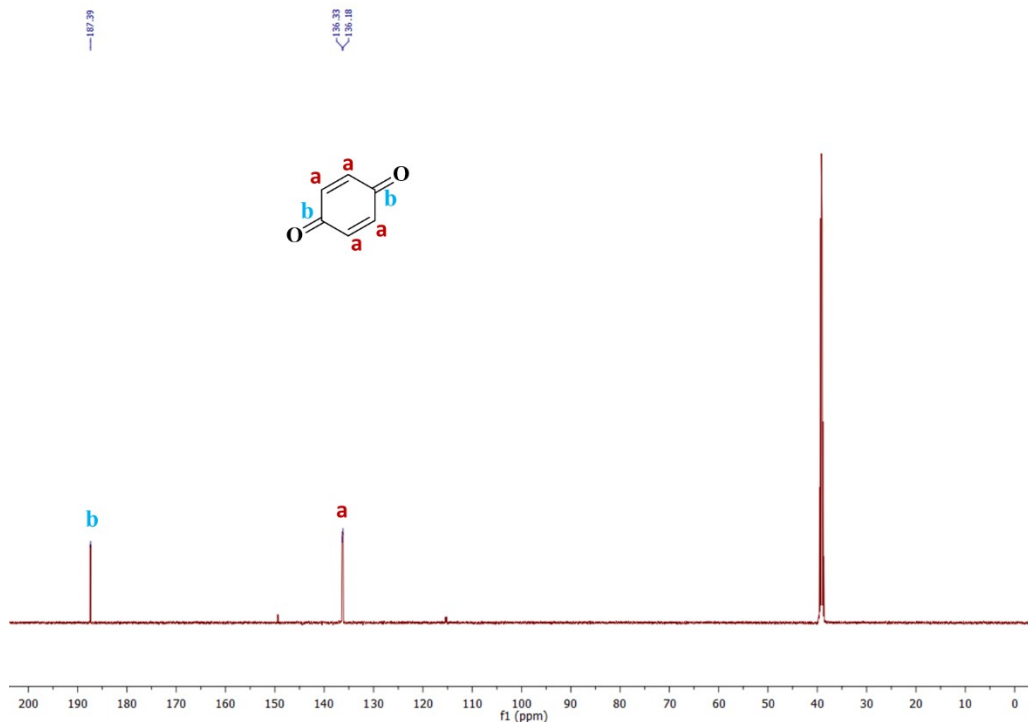
Figure S32. ^{13}C NMR spectra of benzoquinone obtained after 3 h of anodic oxidation of phenol at 1.50 V vs RHE potential using Fe-Co(O)OH.
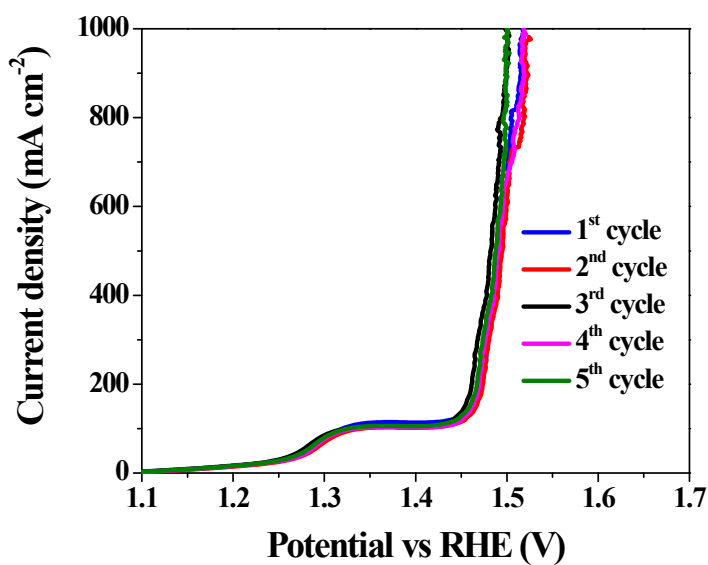

Figure S33. LSV profiles for the five successive cycles of BA oxidation after repeating the CA tests for five times at 1.50 V vs RHE potential using Fe-Co(O)OH.
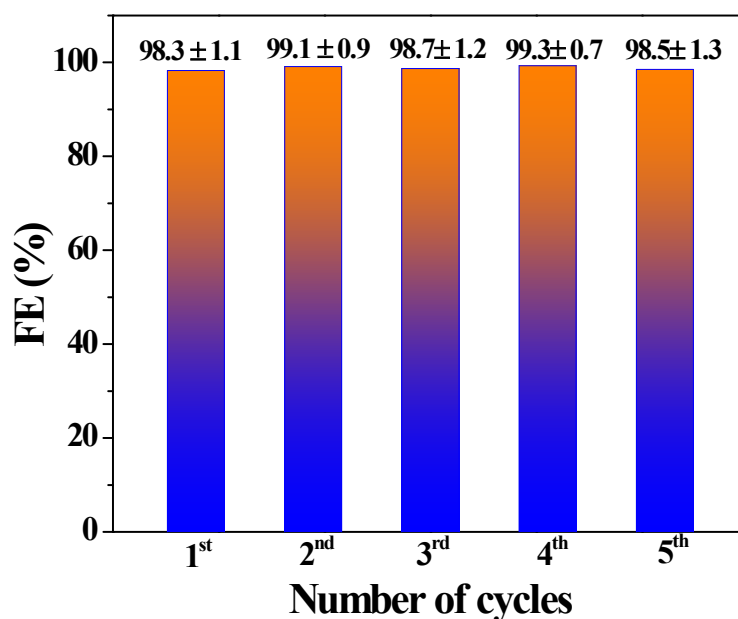
Figure S34. Plot for the FE measurement of the BA oxidation for five successive cycles using Fe-Co(O)OH.

Equation S1.
Calculation of cost and energy efficiency

1. Cost of a catalyst preparation

[Cost of a catalyst] = {cost of [metal precursor/mg] + [ligand/mg] + [nickel foam/piece] + cost of preparation}

Cost of a catalyst film = [2.49 Rs/mg + 1.11 Rs/mg + 10 Rs/piece + 1.23 Rs/film]

Cost of a catalyst film = 14.83 Rs = 0.18 dollar

2. The cost of distilled water utilized for the reaction and electrolyte preparation = 8.1 Rs for 30 mL

For OER

Energy for running water splitting = energy required

$$\text{Energy required} = \frac{\text{Voltage (V) x Current (mA)}}{H_2 \text{ production rate (L/h)}}$$

$$\text{Energy required} = \frac{1.58 \ x \ 50 \ (VmA)}{0.01657 \ (L/h)} = \frac{1.58 \ x \ 50 \ x \ 10^{-3} \ (VA)}{0.01657 \ x \ 10^{-3} \ (m^3/h)}$$

$$= 4767.6 \ Wh/m^3 \ H_2 \ = 4.76 \ kWh/m^3 \ H_2$$

For BA oxidation

$$\text{Energy required} = \frac{\text{Voltage (V) x Current (mA)}}{\text{H}_2 \text{ production rate (L/h)}}$$

$$\text{Energy required} = \frac{1.44 \text{ x } 50 \text{ (VmA)}}{0.05352 \text{ (L/h)}} = \frac{1.44 \text{ x } 50 \text{ x } 10^{-3} \text{ (VA)}}{0.05352 \text{ x } 10^{-3} \text{ (m}^3/\text{h)}}$$

$$= 1345.2 \text{ Wh/m}^3 \text{ H}_2 = 1.34 \text{ kWh/m}^3 \text{ H}_2$$

Table S2. Comparison of the energy efficiency of the Fe-Co(O)OH with the previously reported catalysts.

| Catalyst	Energy efficiency during OER	Energy efficiency during alcohol oxidation	Reference
Fe-Co(O)OH	**4.76 kWh/m^3 H$_2$**	**1.34 kWh/m^3 H$_2$**	**This work**
Ni$_3$P-Cu$_3$P/CF	4.66 kWh/m^3 H$_2$	3.80 kWh/m^3 H$_2$	*Nano Energy*, 2024, **127**, 109727.
NiMoN	5.53 kWh/m^3 H$_2$	2.23 kWh/m^3 H$_2$	*Adv. Funct. Mater.*, 2024, 2407601.
NiVRu-LDH	5.14 kWh/m^3 H$_2$	4.62 kWh/m^3 H$_2$	*Adv. Mater.*, 2023, **35**, 2300935.
Metallic-Cu	5.00 kWh/m^3 H$_2$	0.35 kWh/m^3 H$_2$	*Nat. Catal.* 2022, **5**, 66-73.
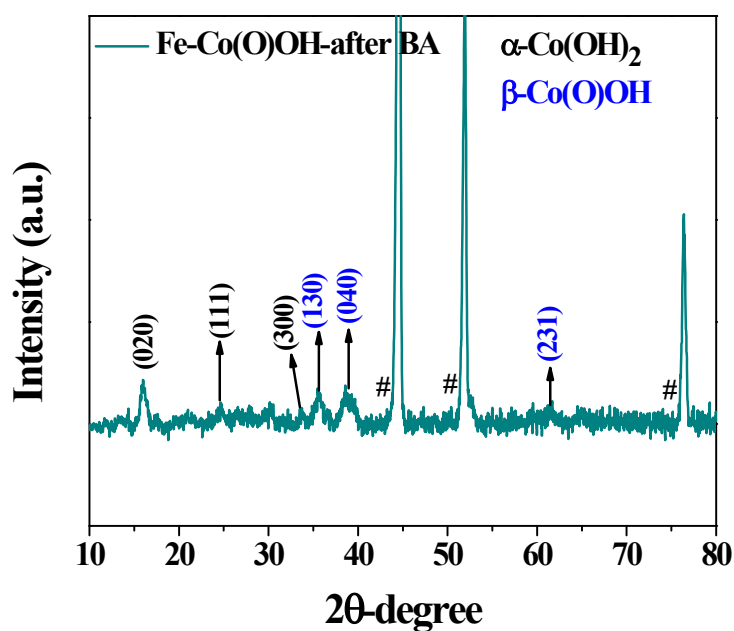
Figure S35. PXRD pattern of Fe-Co(O)OH-BA after 3 h of benzyl alcohol oxidation. The PXRD peaks were well indexed and assigned for the mixed phase of α-Co(OH)$_2$ (JCPDF No.-48-0083) and β-Co(O)OH (JCPDF No.-26-0480).
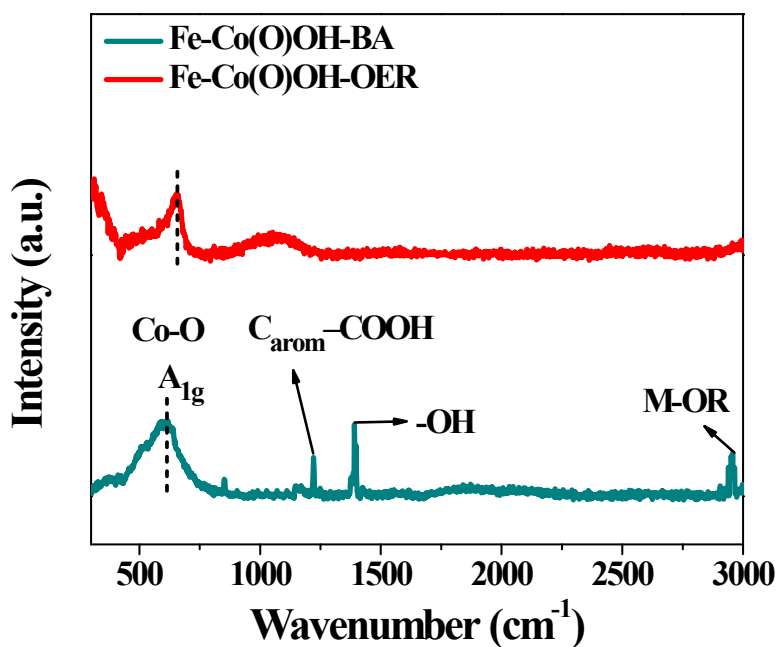

Figure S36. Raman spectra of Fe-Co(O)OH-OER and Fe-Co(O)OH-BA (after 3 h of benzyl alcohol oxidation).[9–11]

Explanation of XPS after BA oxidation

The Co 2p XPS of Fe-Co(O)OH-BA was fitted into two peaks at 781.14 eV and 797.00 eV for Co $2p_{3/2}$ and Co $2p_{1/2}$, respectively. The peaks at 779.33 eV and 781.66 eV were corresponded to Co^{3+} and Co^{2+}, respectively. Further, an increase in spin-orbit coupling spacing of Fe-Co(O)OH-BA (15.86 eV) compared to Fe-Co(O)OH-OER (15.20 eV) was also detected. The Co^{3+}/Co^{2+} ratio was found to be lower (2.43) in Fe-Co(O)OH-BA compared to Fe-Co(O)OH-OER (3.12). This result showed that although Fe-Co(O)OH-BA and Fe-Co(O)OH-OER possessed mixed valent Co^{2+}/Co^{3+} and the amount of Co^{2+} is higher in Fe-Co(O)OH-BA. The Fe 2p XP-spectrum of Fe-Co(O)OH-BA was deconvoluted into two peaks at 708.24 eV and 721.23 eV corresponded to Fe $2p_{3/2}$ and Fe $2p_{1/2}$, respectively. The two peaks at 708.47 eV and 709.61 eV indicated the presence of mixed valent Fe^{2+} and Fe^{3+}. Compared to the Fe 2p XPS of fresh Fe-Co(O)OH-OER, a negative shift of 0.47 eV in the Fe $2p_{3/2}$ peak was recorded indicating the mixed valent Fe^{2+}/Fe^{3+} in Fe-Co(O)OH-BA. The O 1s spectrum of Fe-Co(O)OH-BA revealed three peaks (O1) 528.91 eV, (O2) 530.43 eV and (O3) 531.80 eV, assigned for M-O bond, surface –OH and adsorbed water molecules, respectively. A slight shift of the O 1s spectrum of Fe-Co(O)OH-BA towards negative binding energy was observed compared to the Fe-Co(O)OH-OER, attributed to the high electronic density of O-atom in Fe-Co(O)OH.
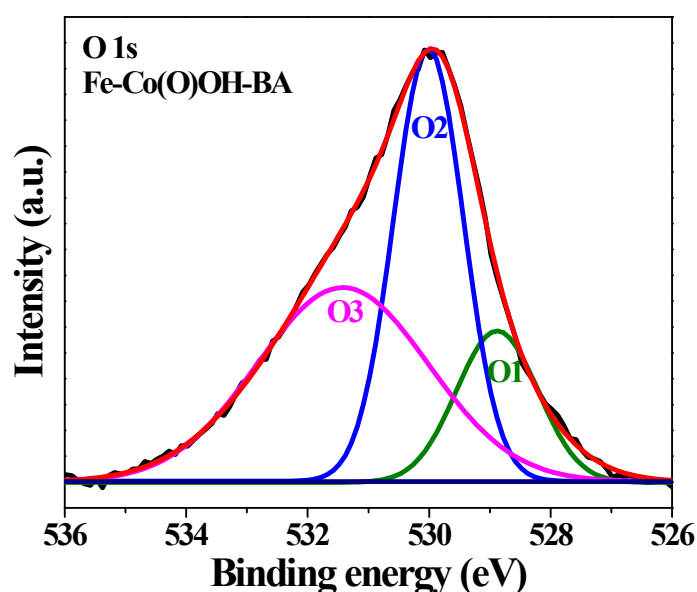

Figure S37. O 1s XPS of Fe-Co(O)OH-BA showing three peaks (O1) 528.85 eV, (O2) 530.03 eV and (O3) 531.80 eV, assigned for the M-O bond, surface –OH and adsorbed water molecules, respectively.[12-15]
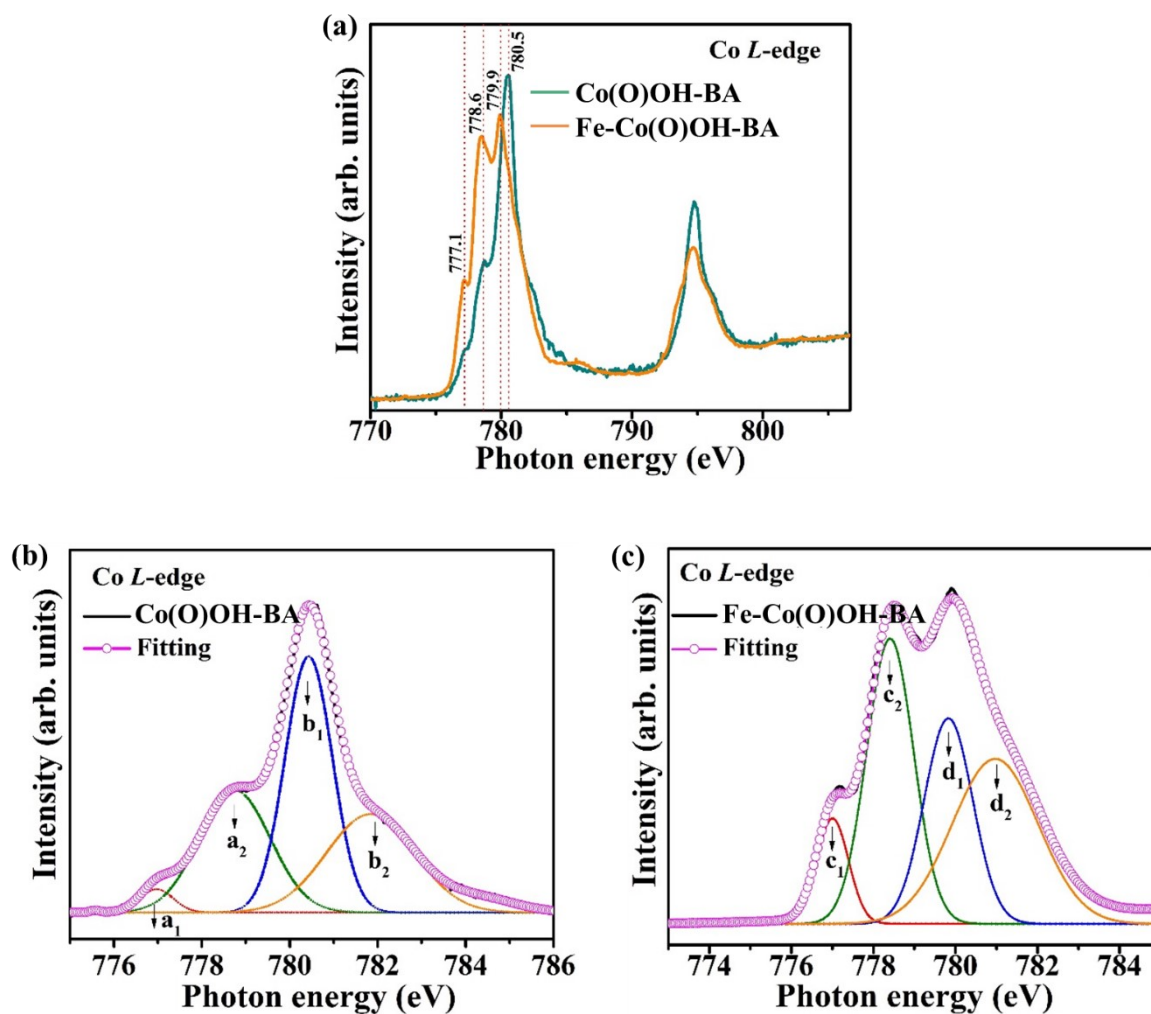
Figure S38. (a) Co L edge spectra of Fe-Co(O)OH-BA and Co(O)OH-BA (after 3 h of benzyl alcohol oxidation); (b) fitting of Co L edge spectra of Co(O)OH-BA and fitting of Co L edge spectra of Fe-Co(O)OH-BA.[12–15]
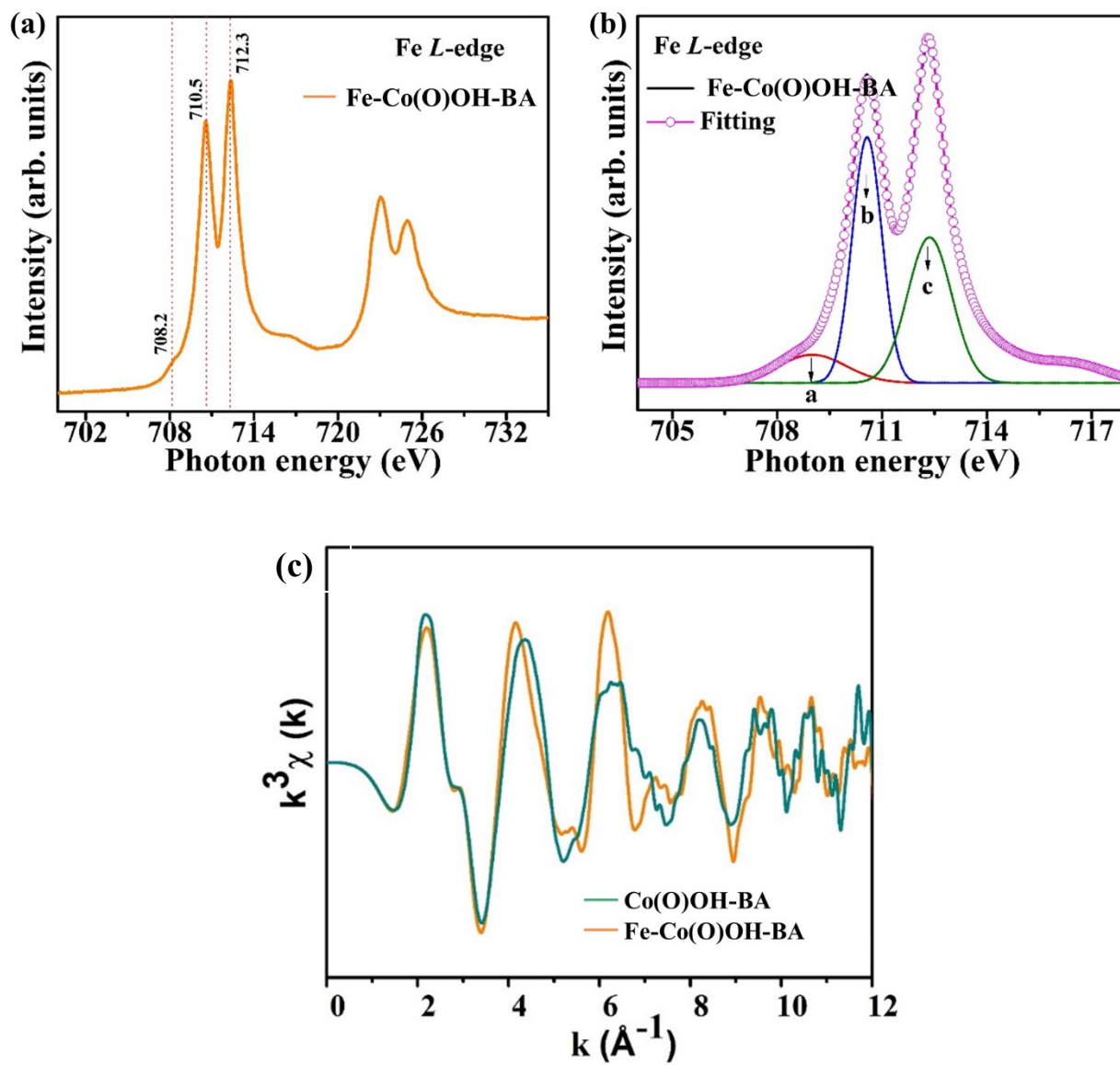
Figure S39. (a) Fe L edge spectra of Fe-Co(O)OH-BA (after 3 h of benzyl alcohol oxidation); (b) fitting of Fe L edge spectra of Fe-Co(O)OH-BA,[16,17] and (c) Fourier transformed k³χ data of the EXAFS oscillations of Co k-space of Co(O)OH-BA and Fe-Co(O)OH-BA.[12–15]
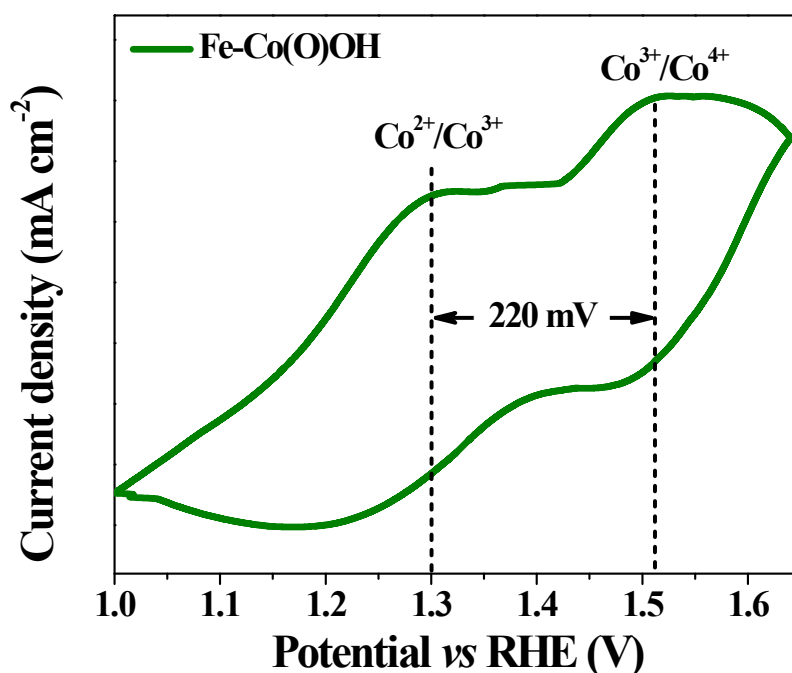
Figure S40. CV profile of Fe-Co(O)OH showing the peaks for the oxidation of Co^{2+}/Co^{3+} and Co^{3+}/Co^{4+}.[11]

Table S3: Details of the synthesized catalysts

Precatalyst	Co/Fe ratio from XPS	Active catalyst	Co/Fe ratio from XPS
CoFe-PBA@NF	1.02	Fe-Co(O)OH-BA@NF	1.22

References

[1] B. Singh, O. Prakash, P. Maiti, P. W. Menezes and A. Indra, *Chem. Commun.*, 2020, **56**, 15036–15039.

[2] B. Singh and A. Indra, *Dalt. Trans.*, 2021, **50**, 2359–2363.

[3] N. Mitschke, S. P. B. Vemulapalli and T. Dittmar, *Environ. Chem. Lett.*, 2023, **21**, 689–723.

[4] K. Yang, Q. Dang, P. Cai, Y. Gao, Z. Yu and X. Bai, *J. Org. Chem.*, 2017, **82**, 2336−2344.

[5] M. Wernerova and T. Hudlicky, *Synlett*, 2010, **18**, 2701-2707.

[6] A. Indra, U. Paik and T. Song, *Angew. Chem. Int. Ed.*, 2018, **57**, 1241–1245.

[7] S. Dutta, H. S. Han, M. Je, H. Choi, J. Kwon, K. Park, A. Indra, K. M. Kim, U. Paik and T. Song, *Nano Energy*, 2020, **67**, 104245.

[8] B. Singh, O. Prakash, P. Maiti and A. Indra, *ACS Appl. Nano Mater.*, 2020, **3**, 6693–6701.

[9] E. Skupien, R. J. Berger, V. P. Santos, J. Gascon, M. Makkee, M. T. Kreutzer, P. J. Kooyman, J. A. Moulijn and F. Kapteijn, *Catalysts*, 2014, **4**, 89–115.

[10] J. Yang, H. Liu, W. N. Martens and R. L. Frost, *J. Phys. Chem. C*, 2010, **114**, 111–119.

[11] A. Moysiadou, S. Lee, C.-S. Hsu, H. M. Chen and X. Hu, *J. Am. Chem. Soc.*, 2020, **142**, 11901–11914.

[12] J. He, Y. Liu, Y. Huang, H. Li, Y. Zou, C.-L. Dong and S. Wang, *Adv. Funct. Mater.*, 2021, **31**, 2009245.

[13] G. van der Laan and I. W. Kirkman, *J. Phys. Condens. Matter*, 1992, **4**, 4189–4204.

[14] D. Carta, M. F. Casula, A. Corrias, A. Falqui, G. Navarra and G. Pinna, *Mater. Chem. Phys.*, 2009, **113**, 349–355.

[15] J.-M. Chen, Y.-Y. Chin, M. Valldor, Z. Hu, J.-M. Lee, S.-C. Haw, N. Hiraoka, H. Ishii, C.-W. Pao, K.-D. Tsuei, J.-F. Lee, H.-J. Lin, L.-Y. Jang, A. Tanaka, C.-T. Chen and L. H. Tjeng, *J. Am. Chem. Soc.*, 2014, **136**, 1514–1519.

[16] S. Chen, Z. Kang, X. Zhang, J. Xie, H. Wang, W. Shao, X. Zheng, W. Yan, B. Pan and Y. Xie, *ACS Cent. Sci.*, 2017, **3**, 1221–1227.

[17] J. Zhou, Y. Hu, Y.-C. Chang, Z. Hu, Y.-C. Huang, Y. Fan, H.-J. Lin, C.-W. Pao, C.-L. Dong, J.-F. Lee, C.-T. Chen, J.-Q. Wang and L. Zhang, *ACS Catal.*, 2022, **12**, 3138–3148.

[18] A. Moysiadou, S. Lee, C. Hsu, H. M. Chen and X. Hu, *J. Am. Chem. Soc.*, 2020, **142**, 11901−11914.